









Phosphate Adsorption from Aqueous Solution Using Different Mass of Raw Waste Marsh Clam Shells as an Alternative Novel Adsorber

Noorul Hudai Abdullah ^{1,*}, Rivahshini Shanmuganathan ¹, Thivnashdewi Muthusamy ¹, Yeoh Zi Hui ¹, Nur Atikah Abdul Salim ², Mohamad Ali Fulazzaky ³, Tony Hadibarata ⁴, Muhammad Noor Hazwan Jusoh ⁴

¹ Neo Environmental Technology, Centre for Diploma Studies, Universiti Tun Hussein Onn Malaysia, Pagoh Education Hub, 84600 Pagoh, Johor, Malaysia

² School of Occupational, Safety and Health, Netherlands Maritime University College (NMUC), 80000 Johor Bahru, Johor, Malaysia

³ School of Postgraduate Studies, Universitas Djuanda, Jalan Tol Ciawi No. 1, Ciawi, Bogor 16720, Indonesia

⁴ Environmental Engineering Program, Faculty of Engineering and Science, Curtin University, CDT 250, Miri 98009, Malaysia

* Correspondence: noorul@uthm.edu.my;

Scopus Author ID 57217560465

Received: 14.11.2023; Accepted: 28.01.2024; Published: 21.07.2024

Abstract: Eutrophication occurs when excess phosphate is released from domestic wastewater, deteriorating the receiving water body. Phosphate pollutants are effectively removed by using chemical treatment in the tertiary wastewater treatment process; however, this method bears a high cost. Hence, this study used waste raw marsh clam shells as an adsorbent to remove phosphate from a synthetic phosphate solution (10 mg/L). The phosphate solution was mixed with the different adsorbent masses (2, 4, 6, 8, and 10 g) with particle sizes ranging from 1.18 to 2.36 mm. The batch experiment data were fitted to kinetic and isotherm adsorption models. The physicochemical properties of the shells were also analyzed to determine the adsorbent characteristics by using X-ray diffraction (XRD), scanning electron microscopy (SEM), energy dispersive X-ray fluorescence (EDXRF), and Fourier transform infrared spectroscopy (FTIR). In this study, the highest phosphate removal efficiency from solution was 51.67% in 10 g of raw adsorbent, where the high amount of adsorbent increased phosphate removal efficiency from the solution due to the high number of active sites on the adsorbent surface. The data fitted well with a pseudo-second-order kinetic model where the R^2 value was 0.9989, demonstrating that the adsorption process is a chemisorption. Meanwhile, the analysis of the isotherm model shows that the Freundlich model ($R^2 = 0.7322$) is the best model to represent phosphate adsorption onto marsh clam shell, showing that the adsorbent surface is heterogeneous. In a nutshell, raw marsh clam shell has been proven to be an excellent adsorbent material for removing phosphate from wastewater.

Keywords: marsh clam shell; eutrophication; kinetic; isotherm; phosphate.

© 2024 by the authors. This article is an open-access article distributed under the terms and conditions of the Creative Commons Attribution (CC BY) license (<https://creativecommons.org/licenses/by/4.0/>).

1. Introduction

Malaysia is a developed country that implements an open economy, and the rapid development generates a combined volume of wastewater from industrial and municipal sectors of approximately 2.97 billion cubic meters per year [1]. Thus, wastewater treatment must be done in an effective way to secure the water resources and the environment. Improper

wastewater treatment, such as phosphorus pollutants, could affect the ecosystem and human health. The phosphate sources are detergent, fertilizer, manure, and factory activities. Excessive phosphate concentration in water bodies caused by human activities is known to reduce water quality by eutrophication, stimulating algal growth and negatively impacting aquatic environments. By hastening eutrophication, this degradation of the receiving water has caused major environmental concerns, particularly in the water ecosystem, endangering aquatic life and human health worldwide in recent decades [2]. More than 60% of the 90 main lakes are being eutrophicated in Malaysia [3].

In this study, an environmentally friendly approach was applied to remove phosphates from water. Chemical and biological treatment methods have several disadvantages, including expensive chemical costs and a long start-up time, making them a slow procedure [4]. On the other hand, adsorption is the most capable technique for removing phosphate from water because of its easy operation, low cost, and high effectiveness [5]. Marine shell wastes can be used as adsorbents for phosphate removal as they are available in large quantities, and many of them are landfilled [6]. This study uses a natural adsorbent, the marsh clamshell, to adsorb phosphate. Waste marsh clam shells with leftovers produce major odor pollution and necessitate a large land area for landfilling due to the lack of a suitable disposal method. This abandoned waste can be transformed into a valuable adsorbent product for a sustainable world. This study aims to investigate the performance of phosphate removal in solution with different masses of raw waste marsh clam shells in a batch experiment. The data was verified using kinetic and isotherm adsorption models to evaluate the interaction between the solution and the adsorbent. The discovery of a new adsorbent material derived from trash to extract phosphates from an aqueous solution exemplifies the research's uniqueness, which has potential implementation for tertiary wastewater treatment in the future.

2. Materials and Methods

2.1. Preparation of the adsorbent.

The waste marsh clam shells were collected from Bachok, Kelantan, Malaysia. The shells were cleaned with tap water and deionized water several times. After that, the shells were dried under the sun for 2 days and dried in the laboratory oven at 30°C for 2 days. The dried shells were then crushed using a mortar and pestle. The granular shell powder was then sieved with a sieve shaker to get particles in the 1.18–2.36 mm range. The sieved shell powder was weighed (2, 4, 6, 8, and 10 g) and packed into plastic containers.

2.2. Preparation of aqueous solution.

The aqueous solution was prepared by dissolving 0.1433 g potassium dihydrogen phosphate in 1 L deionized water to produce 100 mg/L phosphate solution. The stock solution was then diluted to produce a 10 mg/L phosphate solution.

2.3. Batch adsorption experiment.

Five batches of experiments were conducted, each with a different mass (2, 4, 6, 8, 10 g) of adsorbent. The batch experiments were carried out at room temperature with a concentration of 10 mg/L of phosphate solution. A 100 mL phosphate solution volume was added to 10 conical flasks, and the adsorbents were added. The conical flasks were shaken at

170 rpm by using an orbital shaker according to their fixed time. The fixed times for each batch were 30, 60, 120, 180, 300, 420, 1440, 2880, 4320, and 5760 min. The solution was taken out at the specified time and filtered with a strainer. The residual adsorbent on the strainer was dried for physicochemical characterizations. The solution was then filtered again with a vacuum pump and filter paper to determine the extractable phosphate concentrations. The filtered solution was measured using a UV-vis spectrometer (HACH DR6000) and the reactive amino acid method.

The adsorption capacity and removal efficiency for each batch experiment were calculated after the initial and final concentrations had been recorded. Their formulas are shown in **Eq. 1** and **Eq. 2**, respectively [7].

$$q = \frac{C_i - C_f}{m} \times V \quad (1)$$

$$E = \frac{C_i - C_f}{C_i} \times 100\% \quad (2)$$

where C_i = initial phosphate concentration (mg/L), C_f = final phosphate concentration (mg/L), m = mass of adsorbent (g), and V = volume of solution (L).

2.4. Characteristics of marsh clam shell.

The shell's surface morphology and elemental composition were investigated using a scanning electron microscope (SEM; COXEM EM-30AX PLUS). FTIR spectrometer (Perkin Elmer Spectrum Two) was used to carry out FTIR analysis to determine the functional groups of the shell before and after adsorption [8]. X-ray diffraction (XRD) analysis was performed to identify the mineral structure of the shell by using an X-ray diffractometer (Second Generation BRUKER D2 Phaser Benchtop XRD).

2.5. Adsorption kinetics and isotherms models.

Pseudo-first-order and pseudo-second-order kinetic models were applied in this study to verify the experimental data. Adsorption kinetics is the study of adsorption uptake over time at constant pressure or concentration, and it is used to assess adsorbate diffusion in pores [9]. The pseudo-first-order equation can be described as **Eq. 3**.

$$\ln[q_e - q(t)] = \ln q_e - k_1 t_i \quad (3)$$

The pseudo-second-order equation can be expressed as **Eq. 4**.

$$\frac{t_i}{q_t} = \frac{1}{k_2 q_e^2} + \frac{t_i}{q_e} \quad (4)$$

where q_e = amount of adsorbate adsorbed at equilibrium, q_t = amount of adsorbate at adsorption time, k_1 = pseudo-first-order rate constant, k_2 = pseudo-second-order rate constant, and t_i = time of adsorption.

Adsorption isotherm expresses the relation between the equilibrium of adsorbate concentrations in the liquid phase and the adsorbate amount in the solid phase at a given temperature [10]. The Langmuir and Freundlich models were applied to verify the data. Freundlich isotherm represents a multilayer adsorption process that occurs on heterogeneous surfaces [11]. Meanwhile, the Langmuir model demonstrates a monolayer adsorption process on the adsorbent with a uniform structure and assumes that all the active sites are equivalent and independent [12]. The Freundlich model is defined as **Eq. 5**.

$$\ln q_e = \ln K_F + \frac{1}{n} \ln C_e \quad (5)$$

The Langmuir model is represented as **Eq. 6** [13].

$$\frac{1}{q_e} = \frac{1}{k_L q_{max} C_e} + \frac{1}{q_{max}} \quad (6)$$

where q_e = amount of adsorbate adsorbed at equilibrium, K_F = Freundlich adsorption constant, C_e = equilibrium solution concentration of the adsorbate, n = empirical constant, q_{max} = maximum adsorption ability, C_e = concentration of adsorbate at equilibrium, and K_L = Langmuir constant.

3. Results and Discussion

3.1. Characterisation of samples.

The SEM photographs showing the surface morphology of the marsh clam shell with magnifications of 1500×, 5000×, and 10000× are illustrated in Figure 1. Figure 1(a) shows the SEM image of 1500× magnification, where the clamshell has a compact texture. There are many small and irregular rough pores on the outer surface, indicating that it has strong structural stability [14].

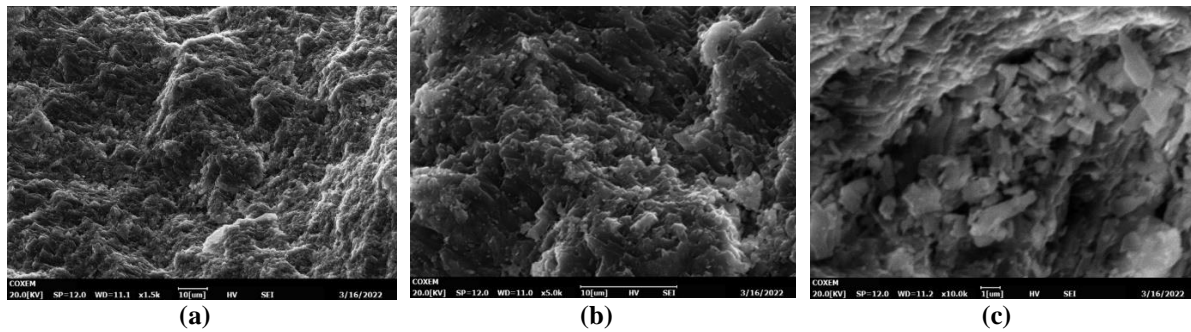


Figure 1. SEM images for (a) 1500× magnification; (b) 1500× magnification; (c) 10000× magnification.

The chemical compositions of the raw marsh clam shell were identified by energy-dispersive X-ray fluorescence and are shown in Table 1. O (46.13%) and Ca (38.48%) are the major compositions, followed by C (9.52%). The minor compositions are Au (4.06%), Al (1.44%), Sr (0.17%), Mg (0.15%), and Na (0.06%). The abundance of Ca gives the marsh clam shell its potential to bind with phosphate to remove it from the aqueous solution [15].

Table 1. Compositions of marsh clam shell by EDXRF.

Element	Weight (%)
O	46.13
Ca	38.48
C	9.52
Au	4.06
Al	1.44
Sr	0.17
Mg	0.15
Na	0.06

The FTIR spectra (Figure 2) of phosphate adsorbed onto marsh clam shell were recorded from 700 to 1800 cm^{-1} and were compared with each other to obtain information on the modifications and surface functional groups [16]. The position and shape of the phosphate stretching band in the FTIR spectra of the marsh clam shell are influenced by the nature and position of the surface functional groups. The tetrahedral phosphorus molecules are coordinated. Before the phosphate adsorption, the two bands observed at 862.35 and 712.69 cm^{-1} confirm the presence of aragonite [17]. Three shifted bands have a significant change from 712.69, 862.35, and 1476.79 cm^{-1} before adsorption to 712.34, 859.92, and 1449.76 cm^{-1} ,

respectively, after adsorption of the phosphate from aqueous solution onto the marsh clam shell.

The difference in the frequency spectrum of 27.03 cm^{-1} ($1476.79 - 1449.76\text{ cm}^{-1}$) is because the C–C stretching bands at the surface of the marsh clam shell are affected by the asymmetric stretching mode of vibration for the phosphate group [18]. The phosphate molecules adsorbed onto the surface of the marsh clamshell may have influenced C–Cl bending and increase the frequency spectrum by 0.35 cm^{-1} ($712.69 - 712.34\text{ cm}^{-1}$), and 2.43 cm^{-1} ($862.35 - 859.92\text{ cm}^{-1}$) due to ion exchange between the phosphate and C–H functional group. This can affect the stretching because of the vibrations [19]. After the adsorption of phosphate from the aqueous solution onto the marsh clamshell, a new peak was observed at 1787.02 cm^{-1} and could be associated with the stretching vibration onto the surface of the marsh clam shell on C–O, indicating that dihydric phosphate was generated [20].

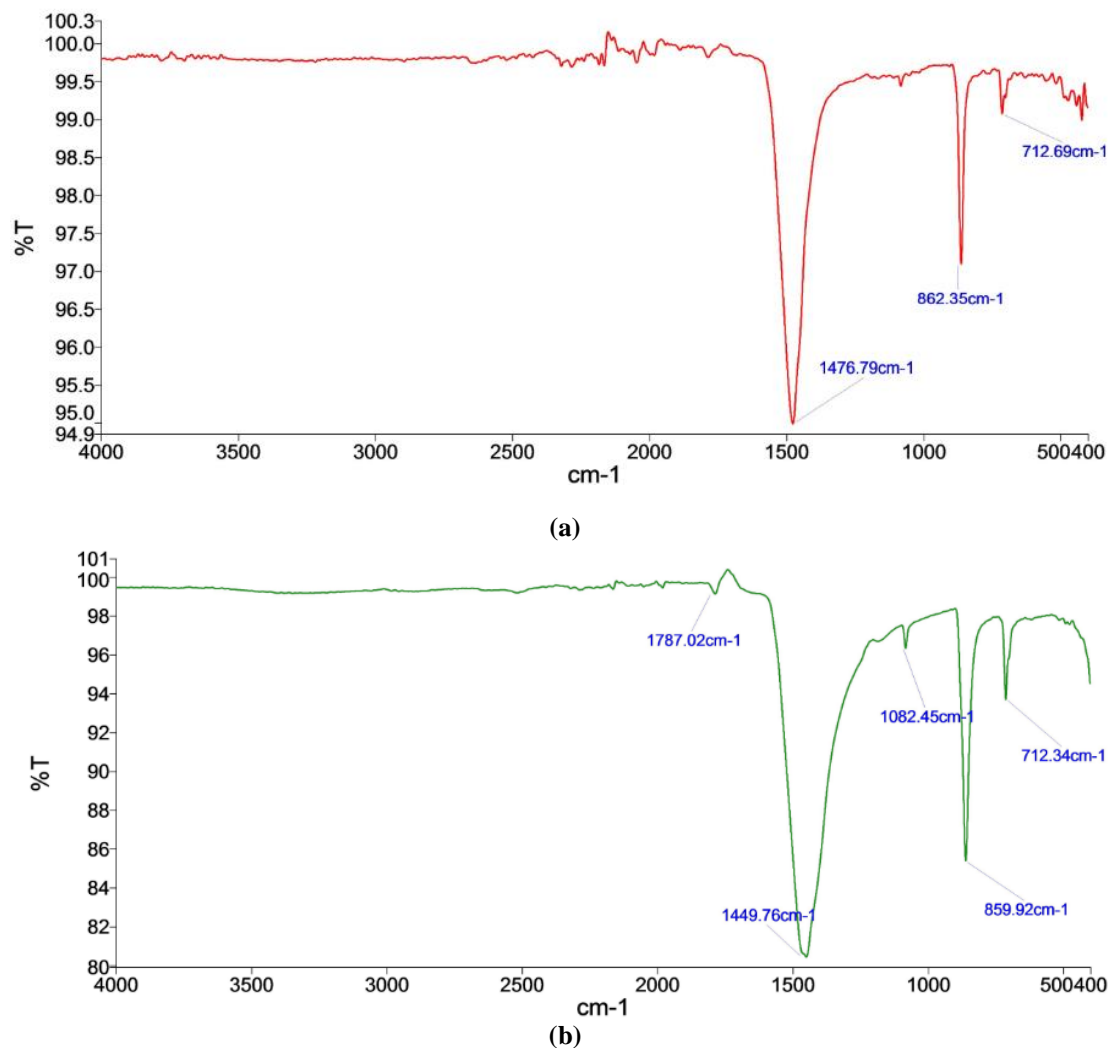


Figure 2. FTIR spectra of marsh clam shell (a) before; (b) after adsorption experiment.

The XRD pattern (Figure 3) of the marsh clamshell sample indicates that aragonite (CaCO₃) is the major component of marsh clam shells. The other components listed on the XRD pattern are calcium oxide (CaO), sodium oxide (Na₂O), and iron oxide (Fe₂O₃).

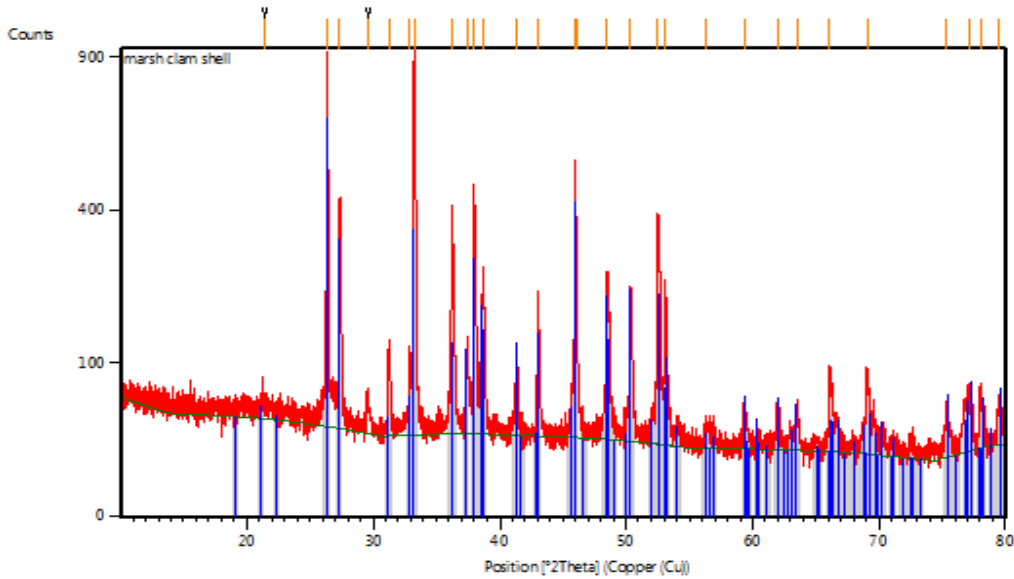


Figure 3. XRD diffraction patterns of marsh clam shell.

3.2. Adsorption capacity, q (mg/g) and removal efficiency, E (%) of phosphate.

The results show that with higher adsorption capacity, the marsh clam shell took longer to adsorb the phosphate.

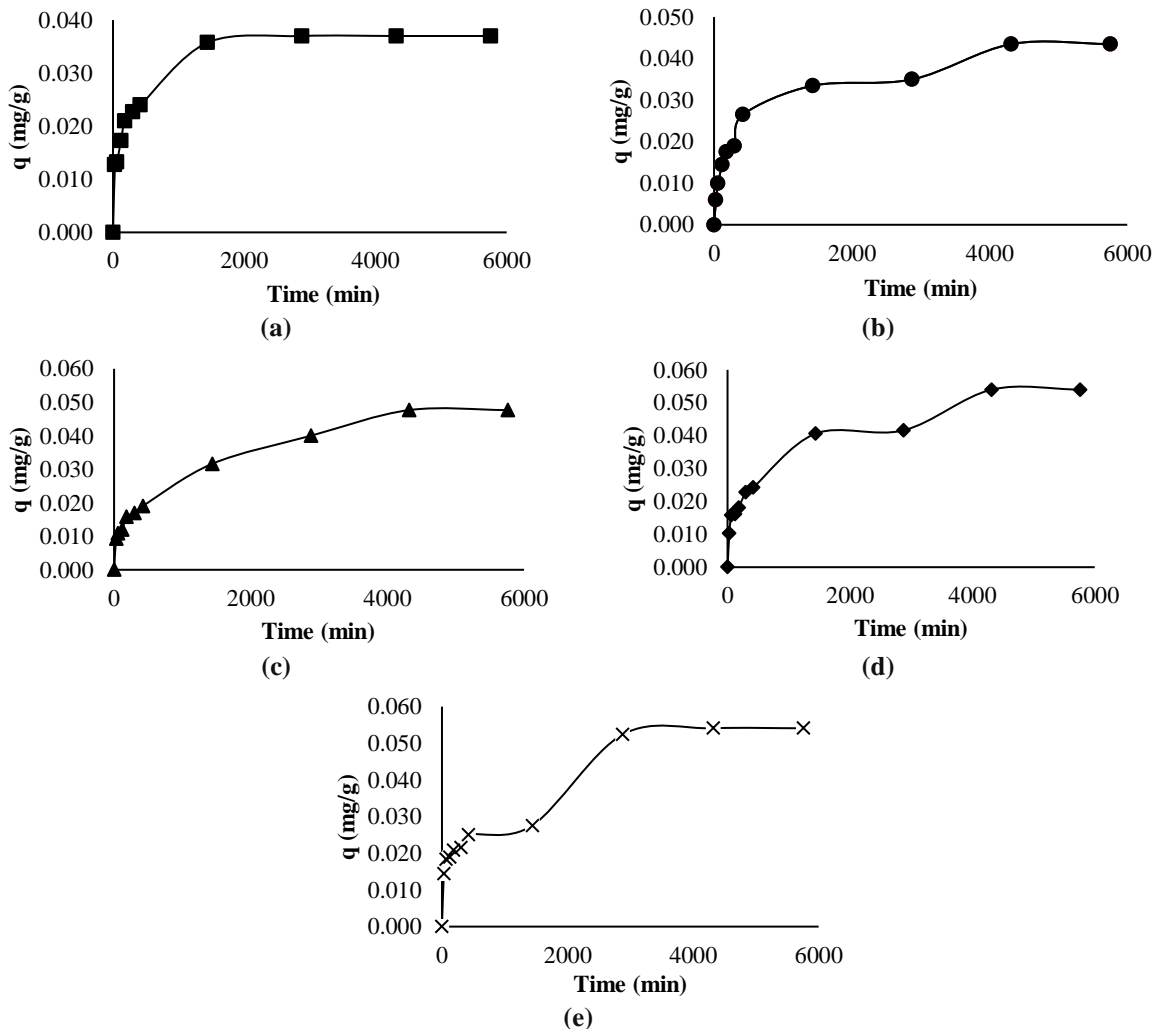


Figure 4. Adsorption capacity, q (mg/g) for different adsorbent masses: (a) 2; (b) 4; (c) 6; (d) 8; (e) 10 g.

Figure 4 shows the adsorption capacity of marsh clam shell where the adsorption capacity was rapid at the beginning and gradually increased until the equilibrium state. The longest duration to determine the maximum adsorption capacity of 2, 4, 6, 8, and 10 g of marsh clam shell was set at 5760 min. The q_e value for 2 g was 0.044 mg/g, 4 g was 0.037 mg/g, 6 g was 0.048 mg/g, and for 8 and 10 g was 0.054 mg/g. The highest adsorption capacity was 0.054 mg/g for 8 and 10 g because adsorption capacity increases as more exchange sites are available for the phosphate to adsorb.

The phosphate removal efficiencies (E) for the marsh clam shell dosages of 2, 4, 6, 8, and 10 g were 8.31%, 14.14%, 27.32%, 41.26%, and 51.67% at 5760 min of contact time, as shown in Figure 5. Electrostatic interactions could be the mechanism of the adsorption process. The affinity between calcium oxide and phosphate ions on the surface of the marsh clam shell is particularly strong since both compounds have unique charges that may generate an attractive effect on one another [21]. Throughout the first 30, 60, 120, 180, 300, and 420 min of contact time, the phosphate removal efficiency of marsh clam shell increased rapidly, then progressively rose to its equilibrium level. As a result, the phosphate adsorptions onto marsh clam shell reached equilibrium at 4320 and 2880 min. The sharp increase in phosphate adsorption onto marsh clam shell from an aqueous solution could be explained by the high number of active sites on the adsorbent surface [22]. The small porous surface of marsh clam shell with a high calcium component increases the removal efficiency as the mass of adsorbent increases.

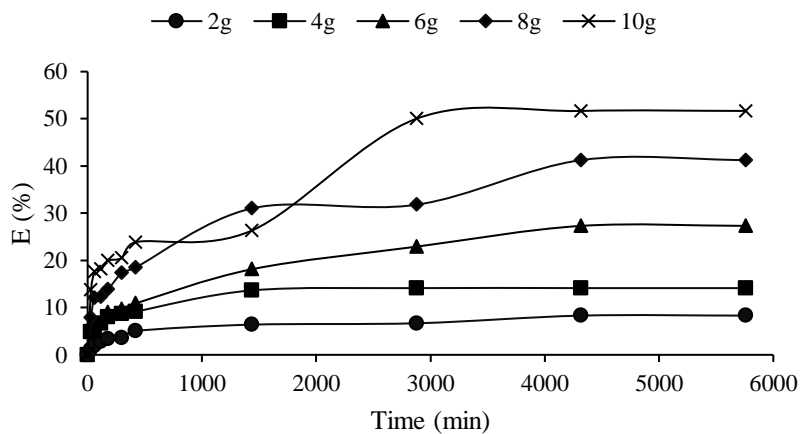


Figure 5. The removal efficiency of various adsorbent masses.

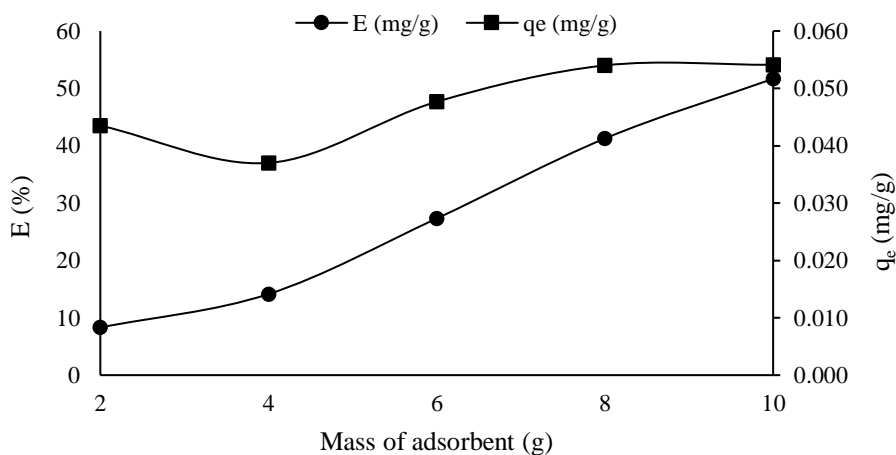


Figure 6. Removal efficiency, E (%), and adsorption capacity, q_e (mg/g) with different raw marsh clam shell masses.

Figure 6 depicts the effect of different amounts of marsh clam shell on E and q during phosphate adsorption. With the increasing amount of marsh clam shell from 2 to 10 g, the value of E for phosphate adsorption increased from 8.31% to 51.67%. The rise in E is related to the high surface area and active sites on the marsh clamshell, allowing it to easily adsorb more phosphate from the aqueous solution until it achieves an equilibrium state, as shown in Figure 6 [23].

3.3. Adsorption kinetic model.

To investigate the mechanism of adsorption and potential rate controlling steps, the kinetic models pseudo-first-order (PFO), pseudo-second-order (PSO), and intraparticle diffusion models were used to test experimental data.

3.3.1. Adsorption kinetics of pseudo-first-order model.

The experimental data from the batch experiment were used to plot $\ln (q_e - q_t)$ versus t. Next, the values of the variables from the PFO model were fitted to the plot to associate the kinetic parameters with the experimental data, as shown in Figure 7. The k_1 and $\ln q_e$ values were evaluated from the slope and intercept of the plot, respectively. The adsorption kinetics follows a PFO model if the plot of $\ln (q_e - q_t)$ versus t gives a straight line [24]. The most appropriate model of PFO should have the smallest F_e value and the highest R^2 value. If the pseudo-first-order model provides a better fit, then the adsorption is a physical process.

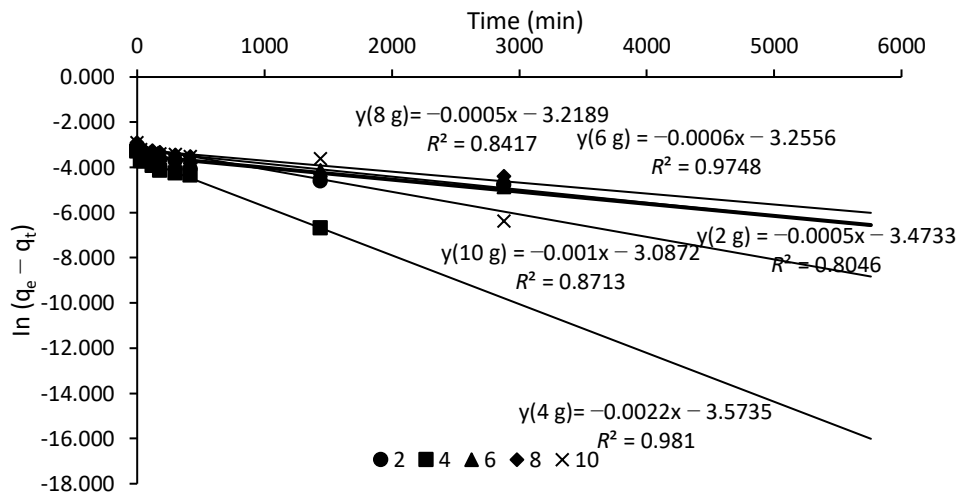


Figure 7. Linear regression analysis for a pseudo-first-order model of phosphate adsorption from aqueous solution.

The values of the PFO parameters q_e (mg/g), k_1 (mg/g), and R^2 were determined by applying the knowledge of the general equation of the straight line, $y = mx + c$. The slope and y-intercept of the straight line are represented by m and c in the general equation, respectively. The y value can be defined as $\ln (q_e - q_t)$, m is defined as k_1 , x is defined as t (time), and c is defined as $\ln (q_e)$. The parameters $q_{e(\text{theory})}$, k_1 , and R^2 were calculated and are shown in Table 2. The best R^2 value is 0.9810 because it is the highest R^2 value with the lowest F_e value, which is 0.1125.

Table 2. The kinetics parameters of the pseudo-first-order model.

Mass (g)	$q_{e(\text{theory})}$	k_1	R^2	F_e	$q_{e(\text{exp})}$
2	0.0310	0.0005	0.8046	0.1579	0.044
4	0.0281	0.0022	0.9810	0.1125	0.037

Mass (g)	$q_e^{(theory)}$	k_1	R^2	F_e	$q_e^{(exp)}$
6	0.0386	0.0006	0.9748	0.1157	0.048
8	0.0400	0.0005	0.8417	0.1764	0.054
10	0.0456	0.0010	0.8713	0.1263	0.054

3.3.2. Adsorption kinetics of pseudo-second-order model.

The experimental data from the batch experiment for the five different adsorbent masses were used to plot t/q_t versus time. The values of the variables in PSO were fitted to the plot, as shown in Figure 8. The values of k_2 and q_e were evaluated from the intercept and slope of the plot, respectively. The adsorption kinetics follows a PSO model if the plot of t/q_t versus t gives a straight line. If the PSO model fits the experimental data better, the adsorption is chemical [25].

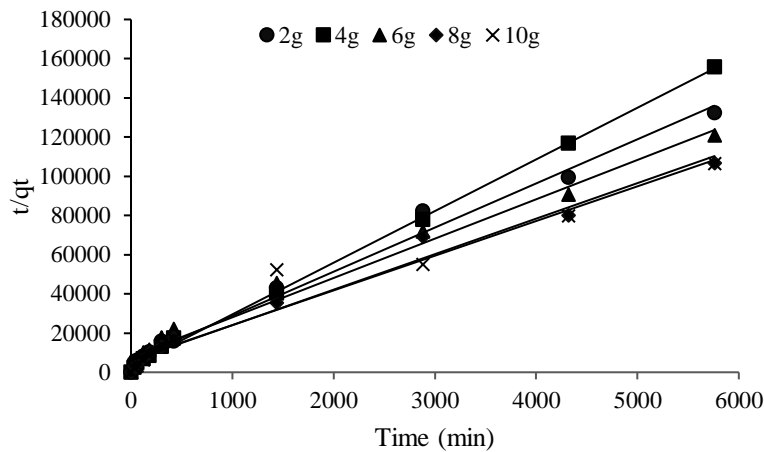


Figure 8. Linear regression analysis for a pseudo-second-order model of phosphate adsorption from aqueous solution.

The values for the PSO parameters t_i/q_t , $1/q_e$, and $1/k_2q_e^2$ were obtained by comparing them with the general equation of a straight line. The m and c in the general equation are equal to $1/c$ and $1/k_2q_e^2$, respectively. The x and y values represent t (time) and t_i/q_t , respectively. Then, the parameters $q_e^{(theory)}$, k_2 , and R^2 were determined based on the plot and are displayed in Table 3.

Table 3. The kinetics parameters of the pseudo-second-order model

Mass (g)	$q_e^{(theory)}$	k_2	R^2	F_e	$q_e^{(exp)}$
2	0.0444	0.0810	0.9891	0.0247	0.0435
4	0.0379	0.2197	0.9989	0.0245	0.0370
6	0.0498	0.0507	0.9827	0.0418	0.0477
8	0.0552	0.0557	0.9822	0.0497	0.0540
10	0.0565	0.0493	0.9599	0.0688	0.0541

Based on the comparison of the correlation coefficient between the R^2 values shown in Table 2 and Table 3, it can be concluded that the adsorption mechanism follows the PSO model as it has a higher value of R^2 (0.9989) and a lower value of F_e (0.0245) compared to the correlation coefficient of PFO ($R^2 = 0.9810$). As a result, the adsorption can be classified as chemisorption, which involves sharing electrons between the marsh clam shell and the phosphate in the aqueous solution [26]. F_e is the error function, and it was used to select the most appropriate model for adsorption because it quantifies the distribution of the adsorbent by providing a mathematical analysis of the results and, most importantly, to verify the consistency of the experimental results, which led to the generation of the adsorption isotherm [27].

3.4. Adsorption isotherm model.

The experimental data for the adsorption of phosphate onto marsh clam shell from aqueous solution were analyzed using the linearised forms of the Freundlich and Langmuir models. All the values of the parameters were calculated using these two isotherm models. The best-fitted isotherm model can be identified from isotherm constants and R^2 values obtained by matching experimental data with the Langmuir and Freundlich models.

3.4.1. Adsorption isotherm of Freundlich model.

The data from the Freundlich model were used to plot a fitting line, as shown in Figure 9. The general equation of a straight line was used to obtain the parameter values of the K_f , $1/n$, and R^2 . By comparing the general equation with the Freundlich equation, the line gradient represents the $1/n$ value while the y-intercept represents the K_f value.

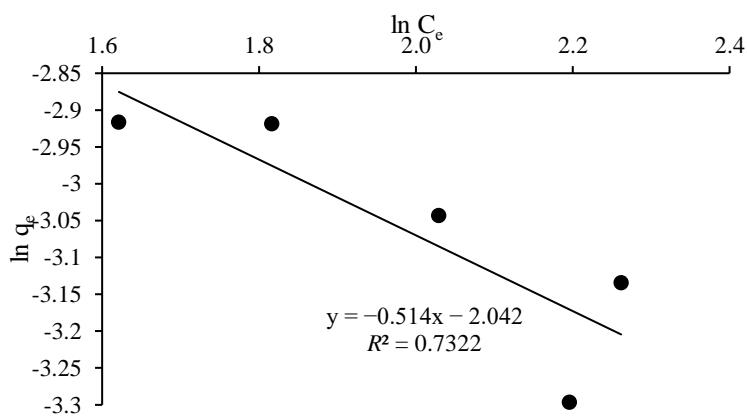


Figure 9. Linear plot of $\ln(q_e)$ versus $\ln(C_e)$ for phosphate adsorption onto raw marsh clamshell from aqueous solution.

3.4.2. Adsorption isotherm of Langmuir model.

The Langmuir adsorption isotherm represents the surface as homogeneous, providing zero lateral contact between adjacent adsorbed molecules. From the data fitted to the Langmuir isotherm model, the value of $1/q_e$ drops as the value of $1/C_e$ grows. The linear interaction between the parameters in the Langmuir model is shown in Figure 10 for raw marsh clam shells.

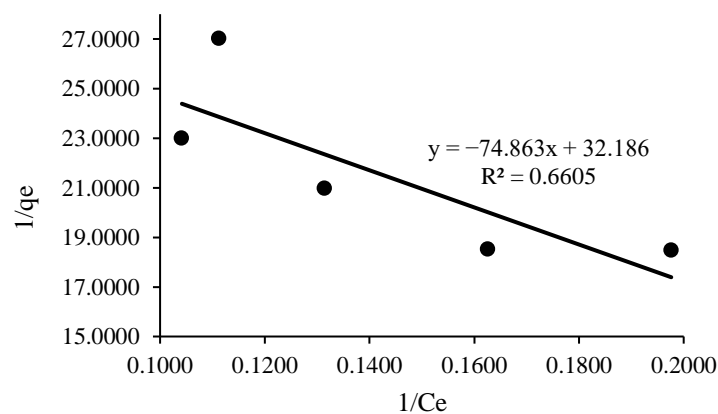


Figure 10. Linear plot of $1/q_e$ versus $1/C_e$ for phosphate adsorption onto marsh clam shell from aqueous solution.

The Freundlich and Langmuir isotherm models can use the nonlinear form translated into linear form equations to determine the relationship between equilibrium concentration and adsorbent quantity. Table 4 shows the parameters for the Freundlich and Langmuir isotherm models.

Table 4. Parameters for the Freundlich and Langmuir isotherm models.

Freundlich Model			Langmuir Model		
n	K _F	R ²	q _{max}	K _L	R ²
-1.94553	0.1298	0.7322	0.0311	-0.42993	0.6605

Based on Table 4, the better correlation coefficient, R^2 was obtained for the Freundlich model, which was 0.7322, compared to that of the Langmuir model, which was 0.6605. The values of energy of adsorption, K_F , and K_L for the Freundlich and Langmuir models were 0.1298 and -0.42993 , respectively. According to the parameter, the Freundlich model has a greater correlation coefficient compared to the Langmuir model because its value of R^2 is closer to 1. Hence, heterogeneous and multilayer sorption was confirmed to be the adsorption process. The adsorption of phosphate occurs on the heterogeneous site of the marsh clam shell with multilayer adsorption, where the adsorbed phosphate on the marsh clamshell surface can attract more phosphate from the aqueous solution [28]. This result implies that active sites with the highest binding energies would be used first for less heterogeneous surfaces and then pursued by weaker sites for more heterogeneous surfaces [29]. The highest component of Ca and microporous marsh clam shell are suitable and efficient for this multilayer adsorption process [30].

4. Conclusions

This study used raw waste marsh clam shell to remove phosphate from aqueous solution using adsorption. The removal efficiency and adsorption capacity of raw waste marsh clam shells towards phosphate in aqueous solution were identified. The experimental data were fitted with kinetic and isotherm adsorption models and verified. The rough surface of raw marsh clam shell with small pores gives it the potential to remove phosphate from wastewater. The highest removal efficiency was 51.67% for 10 g of adsorbent mass due to the high amount of active surface sites on the adsorbent. The data fitted well with the pseudo-second-order kinetic model with an R^2 value of 0.9989 and the lowest F_e value, demonstrating that the adsorption process is a chemisorption. The phosphate adsorption onto raw waste marsh clamshell is also best represented by the Freundlich model with an R^2 value of 0.7322, showing that the adsorbent surface is heterogeneous. The adsorption mechanism suggests that Ca mainly adsorbs phosphate on the surface of a marsh clam shell. The current study shows that waste marsh clam shells could be a viable adsorbent for phosphate removal from wastewater and contribute significantly to environmental quality improvement.

Funding

This research was supported by the Ministry of Higher Education (MOHE) through the Fundamental Research Grant Scheme (FRGS/1/2020/TK0/UTHM/02/27) or Vot No. K308.

Acknowledgments

The authors would also like to thank the Neo Environment Technology (NET), Centre for Diploma Studies (CeDS), Research Management Centre, and Universiti Tun Hussein Onn Malaysia for their support.

Conflicts of Interest

The authors declare no conflict of interest.

References

1. Al-Hazmi, H.E.; Mohammadi, A.; Hejna, A.; Majtacz, J.; Esmaeili, A.; Habibzadeh, S.; Saeb, M.R.; Badawi, M.; Lima, E.C.; Maĳinia, J. Wastewater reuse in agriculture: Prospects and challenges. *Environ. Res.* **2023**, *236*, 116711, <https://doi.org/10.1016/j.envres.2023.116711>.
2. Nguyen, M.-K.; Lin, C.; Nguyen, H.-L.; Le, V.-R.; Kl, P.; Singh, J.; Chang, S.W.; Um, M.-J.; Nguyen, D.D. Emergence of microplastics in the aquatic ecosystem and their potential effects on health risks: The insights into Vietnam. *J. Environ. Manag.* **2023**, *344*, 118499, <https://doi.org/10.1016/j.jenvman.2023.118499>.
3. Derakhshan, A.; Kalantari, R.R.; Farzadkia, M.; Tiyyuri, A.; Esrafil, A. The effect of biological treatment methods on the concentration of carbonaceous pollutants in the slaughterhouse wastewater: A systematic review. *Case Stud. Chem. Environ. Eng.* **2023**, *8*, 100451, <https://doi.org/10.1016/j.cscee.2023.100451>.
4. Shi, Z.; Tan, X.; Li, Y.; Sheng, Y.; Zhang, Q.; Xu, J.; Yang, Y. A novel fungal-algal coupling system for slaughterhouse wastewater treatment and lipid production. *Bioresour. Technol.* **2023**, *387*, 129585, <https://doi.org/10.1016/j.biortech.2023.129585>.
5. Elkhilifi, Z.; Lahori, A.H.; Shahib, I.I.; Iftikhar, J.; Wang, S.; He, L.; Meili, L.; Gendy, E.A.; Sharma, P.; Chen, Z. Comparative assessment of phosphate adsorption properties and mechanisms on Mg/Al-engineered sewage sludge biochar in aqueous solution. *J. Water Process Eng.* **2023**, *56*, 104443, <https://doi.org/10.1016/j.jwpe.2023.104443>.
6. Ngeno, E.C.; Mbuci, K.E.; Necibi, M.C.; Shikuku, V.O.; Olisah, C.; Ongulu, R.; Matovu, H.; Ssebugere, P.; Abushaban, A.; Sillanpää, M. Sustainable re-utilization of waste materials as adsorbents for water and wastewater treatment in Africa: Recent studies, research gaps, and way forward for emerging economies. *Environ. Adv.* **2022**, *9*, 100282, <https://doi.org/10.1016/j.envadv.2022.100282>.
7. Huang, W.; Xu, Y.; Chen, N.; Cheng, G.; Ke, H. Amino-modified hemp stem for high-capacity adsorption of Cr(VI) from aqueous solution. *J. Environ. Chem. Eng.* **2023**, *11*, 111441, <https://doi.org/10.1016/j.jece.2023.111441>.
8. Diao, H.; Yang, H.; Feng, Q.; Zeng, G.; Tang, Y.; Liu, L.; Xue, Q.; Xia, S.; Wu, Z.; Zhang, Y. Efficient phosphorus recovery utilizing Magnesium-Modified Oil-Based drilling cutting Ash: Unraveling the role of ammonia nitrogen independent of struvite formation. *Sep. Purif. Technol.* **2023**, *327*, 124923, <https://doi.org/10.1016/j.seppur.2023.124923>.
9. Khanjani, M.H.; Sharifinia, M.; Mohammadi, A.R. The impact of microplastics on bivalve mollusks: A bibliometric and scientific review. *Mar. Pollut. Bull.* **2023**, *194*, 115271, <https://doi.org/10.1016/j.marpolbul.2023.115271>.
10. Pap, S.; Gaffney, P.P.J.; Bremner, B.; Turk Sekulic, M.; Maletic, S.; Gibb, S.W.; Taggart, M.A. Enhanced phosphate removal and potential recovery from wastewater by thermo-chemically calcinated shell adsorbents. *Sci. Total Environ.* **2022**, *814*, 152794, <https://doi.org/10.1016/j.scitotenv.2021.152794>.
11. Dong, P.; Jing, X.; Li, Y.; Shen, Y.; Li, Q.; Fang, Q. "Twin Lotus Flower" Adsorbents Derived from LaFe Cyanometallate for High-Performance Phosphorus Removal. *Sep. Purif. Technol.* **2022**, *291*, 120924, <https://doi.org/10.1016/j.seppur.2022.120924>.
12. Pérez, S.; Muñoz-Saldaña, J.; Garcia-Nunez, J.A.; Acelas, N.; Flórez, E. Unraveling the Ca-P species produced over the time during phosphorus removal from aqueous solution using biocomposite of eggshell-palm mesocarp fiber. *Chemosphere* **2022**, *287*, 132333, <https://doi.org/10.1016/j.chemosphere.2021.132333>.
13. You, K.; Yang, W.; Song, P.; Fan, L.; Xu, S.; Li, B.; Feng, L. Lanthanum-modified magnetic oyster shell and its use for enhancing phosphate removal from water. *Colloids Surf. A: Physicochem. Eng. Asp.* **2022**, *633*, 127897, <https://doi.org/10.1016/j.colsurfa.2021.127897>.

14. Jing, X.; Zhang, J.; Li, Y.; Li, Q.; Shen, Y.; Liu, J.; Zhang, S.; Fang, Q. Cyanometallate framework templated synthesis of hierarchically porous La(OH)₃ for High-Efficient and stable phosphorus removal from tailwater. *Chem. Eng. J.* **2023**, *465*, 142789, <https://doi.org/10.1016/j.cej.2023.142789>.
15. Gao, M.; Sun, S.; Qiu, Q.; Zhou, W.; Qiu, L. Enrichment denitrifying phosphorus-accumulating organisms in alternating anoxic-anaerobic/aerobic biofilter for advanced nitrogen and phosphorus removal from municipal wastewater. *J. Water Process Eng.* **2023**, *55*, 104089, <https://doi.org/10.1016/j.jwpe.2023.104089>.
16. Bhattacharya, S.; Talukdar, A.; Sengupta, S.; Das, T.; Dey, A.; Gupta, K.; Dutta, N. Arsenic contaminated water remediation: A state-of-the-art review in synchrony with sustainable development goals. *Groundw. Sustain. Dev.* **2023**, *23*, 101000, <https://doi.org/10.1016/j.gsd.2023.101000>.
17. Huang, Y.; Fan, X.; Wang, H.; Li, Z.; Xiong, D.; Pei, Y. Tuning Mg-Al layered double hydroxides synthesized from the novel ionic liquid-based surfactant-free microemulsion for efficiently phosphate removal in aqueous solutions. *J. Mol. Liq.* **2023**, *382*, 121826, <https://doi.org/10.1016/j.molliq.2023.121826>.
18. Borciani, G.; Fischetti, T.; Ciapetti, G.; Montesissa, M.; Baldini, N.; Graziani, G. Marine biological waste as a source of hydroxyapatite for bone tissue engineering applications. *Ceram. Int.* **2023**, *49*, 1572-1584, <https://doi.org/10.1016/j.ceramint.2022.10.341>.
19. Anandan, D.; Kumar, A.; Jaiswal, A.K. Comparative study of hydroxyapatite synthesized using Schiff base and wet chemical precipitation methods. *J. Mech. Behav. Biomed. Mater.* **2023**, *148*, 106200, <https://doi.org/10.1016/j.jmbbm.2023.106200>.
20. Nandiyanto, A.B.D.; Oktiani, R.; Ragadhita, R. HOW TO READ AND INTERPRET FTIR SPECTROSCOPE OF ORGANIC MATERIAL. *Indones. J. Sci. Technol.* **2019**, *4*, 97-118, <https://doi.org/10.17509/ijost.v4i1.15806>.
21. Ouyang, A.; Xiong, W.; Li, X.; Chen, D.; Zhang, L.; Jiang, P. Occurrence and screening-flotation separation for the beneficiation of rare earth elements and yttrium (REY) in core sediments from the Pacific Ocean. *Mar. Geol.* **2023**, *462*, 107097, <https://doi.org/10.1016/j.margeo.2023.107097>.
22. Kurniawan, T.A.; Lo, W.; Othman, M.H.D.; Liang, X.; Goh, H.H.; Chew, K.W. Influence of Fe₂O₃ and bacterial biofilms on Cu(II) distribution in a simulated aqueous solution: A feasibility study to sediments in the Pearl River Estuary (PR China). *J. Environ. Manag.* **2023**, *329*, 117047, <https://doi.org/10.1016/j.jenvman.2022.117047>.
23. Romar-Gasalla, A.; Rivas-Pérez, I.M.; Paradelo-Núñez, R.; Nóvoa-Muñoz, J.C.; Arias-Estévez, M.; Fernández-Sanjurjo, M.J.; Álvarez-Rodríguez, E.; Núñez-Delgado, A. Phosphorus retention on forest and vineyard soil samples, mussel shell, pine-sawdust, and on pyritic, granitic and waste materials. *Geoderma* **2016**, *280*, 8-13, <https://doi.org/10.1016/j.geoderma.2016.06.003>.
24. Liu, Y.; Li, H.A.; Tian, Y.; Jin, Z.; Deng, H. Determination of the absolute adsorption/desorption isotherms of CH₄ and n-C₄H₁₀ on shale from a nano-scale perspective. *Fuel* **2018**, *218*, 67-77, <https://doi.org/10.1016/j.fuel.2018.01.012>.
25. Pérez, S.; Muñoz-Saldaña, J.; Acelas, N.; Flórez, E. Phosphate removal from aqueous solutions by heat treatment of eggshell and palm fiber. *J. Environ. Chem. Eng.* **2021**, *9*, 104684, <https://doi.org/10.1016/j.jece.2020.104684>.
26. Ali, I.; Asim, M.; Khan, T.A. Low cost adsorbents for the removal of organic pollutants from wastewater. *J. Environ. Manag.* **2012**, *113*, 170-183, <https://doi.org/10.1016/j.jenvman.2012.08.028>.
27. Batool, F.; Akbar, J.; Iqbal, S.; Noreen, S.; Bukhari, S.N.A. Study of Isothermal, Kinetic, and Thermodynamic Parameters for Adsorption of Cadmium: An Overview of Linear and Nonlinear Approach and Error Analysis. *Bioinorg. Chem. Appl.* **2018**, *2018*, 3463724, <https://doi.org/10.1155/2018/3463724>.
28. Almasri, D.A.; Saleh, N.B.; Atieh, M.A.; McKay, G.; Ahzi, S. Adsorption of phosphate on iron oxide doped halloysite nanotubes. *Sci. Rep.* **2019**, *9*, 3232, <https://doi.org/10.1038/S41598-019-39035-2>.
29. Li, L.; Qiao, Q.; Zhou, G.; Qi, Y.; Lim, Z.H.; Chau, F.S.; Zhou, G. Design of an on-chip Fourier transform spectrometer based on waveguide Mach-Zehnder Interferometer and fluidics. *Opt. Commun.* **2020**, *460*, 125103, <https://doi.org/10.1016/j.optcom.2019.125103>.
30. Bouaouina, K.; Barras, A.; Bezzi, N.; Amin, M.A.; Szunerits, S.; Boukherroub, R. Adsorption-reduction of Cr(VI) onto unmodified and phytic acid-modified carob waste: Kinetic and isotherm modeling. *Chemosphere* **2022**, *297*, 134188, <https://doi.org/10.1016/j.chemosphere.2022.134188>.